observed or the reactions producing them.

A question of equal interest is what change occurs in the methanol sample below 150 K to cause this change in behavior. Here also we can offer no definite hypothesis. However, we can point out that solid methanol undergoes a second-order phase transition at 157.4 K (λ transition), wherein the orthorhombic form of methanol (β form) undergoes a transition to a monoclinic form (α form).[30] Hawke and co-workers have studied this phenomenon,[31,32] and they find that some surprising chemical changes accompany this seemingly innocuous phase transition. When methanol is caused to pass through the phase transition (from higher temperatures to lower temperatures, i.e., $\beta \rightarrow \alpha$) hydrogen, carbon monoxide, and methane are produced. There are indications that other products such as formaldehyde and ethylene glycol must also be formed. The evolution of gaseous substances is accompanied by changes in the surface of the solid methanol, from an originally smooth surface to a broken, uneven surface with undulations 1 mm or more in depth. Furthermore, when the methanol transition was viewed in the dark, flashes of white light were observed to occur. The emission of light under these circumstances is referred to as triboluminescence. Triboluminescence is characterized by the fact that it is accompanied by electrical discharges, and Hawke and co-workers found that when methanol was cooled through the $\beta \rightarrow \alpha$ transition a large negative potential (roughly -100 V) was produced. In our experiment to observe the melting point of methanol we observed a change in the appearance of the solid methanol at some temperature below the melting point of methanol. The initially more or less smooth surface of the solid methanol was observed to roil and become rougher. The behavior was compatible with that which would be caused by the evolution of a gas. The temperature at which this occurred was not measured nor was the phenomenon investigated further, but we think it possible that this was the same phenomenon described by Hawke and co-workers. One difference which can be mentioned however was that our phenomenon was observed in going from low to high temperature whereas those reported by Hawke and co-workers involved going from high to low temperatures.

It is quite clear that rather large amounts of energy are somehow involved in this phase transition. The temperature at which it occurs (157.4 K) is quite close to the temperature at which the change of spectrum occurs in our study, and we wonder if these two phenomena are related in some causal manner. It is not impossible to think that since the phase transition causes enough strains in the methanol molecules to effect spontaneous breaking of bonds and generation of electrical discharges and light emission, it may also entail enough strain in the solid methanol structure that the particle bombardment involved in producing our spectra may result in a very extensive bond rupture and chemical reaction. These would, of course, be manifested by a complex spectrum.

Acknowledgment. This work was supported in part by the Division of Research Resources, NIH. We thank Gladys McMilleon for typing this manuscript.

Registry No. Methanol, 67-56-1.

(30) Tauer, K. J.; Lipscomb, W. N. *Acta. Crystallogr.* **1952**, *5*, 606.
(31) Hawke, J. G.; Trout, G. J. *J. Phys. Chem.* **1969**, *73*, 3521.
(32) Trout, G. J.; Moore, D. E.; Hawke, J. G. *Nature (London), Phys. Sci.* **1972**, *235*, 174.

Relationship between the Extractability and the Rate of Transfer of Potassium Ion by Macrocyclic Carriers in Liquid Membrane Systems[1]

Shoichiro Yoshida* and Shigeo Hayano

Contribution from the Institute of Industrial Science, University of Tokyo, Minato-ku, Tokyo 106, Japan. *Received December 2, 1985*

Abstract: The relationship between the extractability and the rate of transfer of potassium ion by macrocyclic carriers was investigated in chloroform membrane systems. The rates of ion uptake, ion release, and ion transport and the liquid–liquid extraction constants were determined for a series of carriers (polynactin, dibenzo-18-crown-6, dicyclohexano-18-crown-6, and 18-crown-6). Kinetic equations for ion uptake and release are developed, and the apparent rate constants were calculated by introducing the experimentally determined extraction constants. The rate constants for the ion release and ion uptake are comparable to each other. For the four macrocyclic carriers employed, the rate of uptake was found to control the overall rate of transport through the liquid membrane. Both the rate of uptake and that of transport depend crucially on the extractability of the metal ion. A systematic analysis of each rate taking the constituent equilibria into account indicates that a macrocyclic ligand which forms a more stable complex with the metal ion and is less hydrophobic is preferable as a mobile carrier in liquid membrane systems.

Active research is recently in progress on the use of macrocyclic compounds as mobile carriers in liquid membrane systems, in view of their capability of highly selective transport of metal ions, particularly of alkali- and alkaline-earth metal ions. In most of the previous works, the ion transport mediated by neutral macrocyclic carriers was evaluated in terms of the overall rate of cation transport through liquid membranes.[2-7] The ion transport, being actually the salt transport when a neutral carrier is employed, consists of four major steps: uptake of a cation and an anion into a membrane phase, diffusion of a metal–carrier complex associated with the anion within the membrane phase, release of the ions into an aqueous phase, and back diffusion of a free carrier. For

(1) Presented at the 10th Symposium on Macrocyclic Chemistry, Provo, Utah, Aug 1985.
(2) Reusch, C. F.; Cussler, E. L. *AIChE J.* **1973**, *19*, 736-740.
(3) Lamb, J. D.; Christensen, J. J.; Izatt, S. R.; Bedke, K.; Astin, M. S.; Izatt, R. M. *J. Am. Chem. Soc.* **1980**, *102*, 3399-3403.
(4) Lamb, J. D.; Christensen, J. J.; Oscarson, J. L.; Nielsen, B. L.; Asay, B. W.; Izatt, R. M. *J. Am. Chem. Soc.* **1980**, *102*, 6820-6824.
(5) Lamb, J. D.; Izatt, R. M.; Garrick, D. G.; Bradshaw, J. S.; Christensen, J. J. *J. Membr. Sci.* **1981**, *9*, 83-107.
(6) Burgard, M.; Jurdy, L.; Park, H. S.; Heimburger, R. *Nouv. J. Chim.* **1983**, *7*, 575-578.
(7) Behr, J. P.; Kirch, M.; Lehn, J. M. *J. Am. Chem. Soc.* **1985**, *107*, 241-246.

0002-7863/86/1508-3903$01.50/0

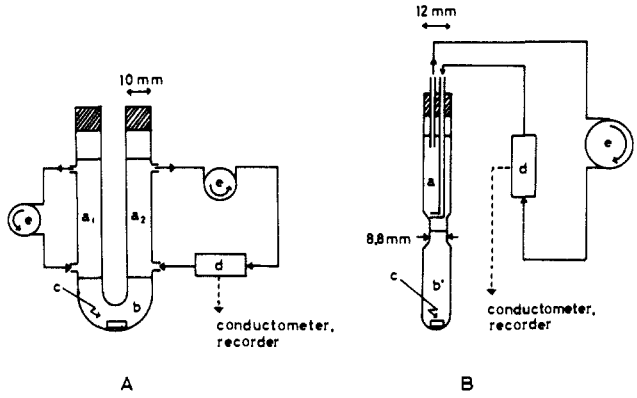

Figure 1. Apparatus for ion transport experiments (A) and for ion-uptake and -release experiments (B). a_1, source aqueous phase; a_2, receiving aqueous phase; b, bulk chloroform membrane; a, aqueous phase; b′, chloroform phase; c, magnetic stirring bar; d, conductivity measuring cell; e, microtube pump.

a better understanding of the ion transport process, or at least for identifying the rate-determining step, it is indispensable to quantify the rates of uptake and release of the ion in question separately. In a previous work, we demonstrated that the overall rate of cation transport is occasionally governed by the rate of release rather than by that of uptake.[8]

It is possible, on the other hand, that the extractability of a metal ion by macrocyclic ligands[9-13] controls the overall ion transport. However, except for a limited number of investigations,[6,7] such a thermodynamic parameter has not been taken explicitly into consideration in analyses of the rate of ion transport through liquid membranes. In the present work, we investigated how the extractability of a metal ion influences the rates of individual steps (uptake, release, and transport) of its transfer through a liquid membrane containing a macrocyclic carrier.

Experimental Section

Reagents. Dibenzo-18-crown-6 (DB18C6), dicyclohexano-18-crown-6 (DC18C6), and 18-crown-6 (18C6) were reagent-grade materials obtained from Merck Chemical Co., Ltd., and were used without further purification. Polynactin (PN) was a gift from the Research Laboratories, Chugai Pharmaceutical Co., Ltd. The PN was a macrotetrolide antibiotic composed of 5% dinactin, 30% trinactin, and 65% tetranactin. Chloroform, picric acid, KOH (Wako-Pure Chemicals Ltd.), and KSCN (Koso Chemical Co., Ltd.) were reagent-grade materials.

Liquid Membrane Experiments. Liquid membrane experiments were performed with a U-shaped glass tube shown in Figure 1A. A membrane solution, chloroform containing a carrier (PN, DB18C6, DC18C6, or 18C6), was stirred at 900 rpm by means of a magnetic stirrer. A source phase (aqueous solution of potassium salt) and a receiving phase (deionized water) were circulated at 15 mL min^{-1} by use of a microtube pump. The whole apparatus was placed in a thermostat controlled at 25 ± 0.2 °C. The changes in the concentration of potassium ion in the two aqueous phases were followed by measuring their electrolytic conductivity. The transport rate (J) was measured 3 times for a given system, and the results were consistent within ±10%.

Ion-Uptake and Ion-Release Experiments. The ion transfer across aqueous/membrane solution interface was examined by using a glass tube illustrated in Figure 1B. In the glass tube were placed 7 g (4.7 mL at 25 °C) of chloroform and 8 mL of water. In ion-uptake experiments, the water contained a potassium salt and the chloroform contained a carrier. In ion-release experiments, the chloroform contained a K^+–carrier complex plus a counteranion and the aqueous phase was deionized water. The stirring of each phase and the measurement of potassium concentration in the aqueous phase were carried out as described above. The chloroform solution of the K^+–carrier complex ion pair used in the ion-release experiments was prepared by solvent extraction.

Solvent Extraction Experiments. The distribution ratios of K^+ at aqueous phase/chloroform interfaces were obtained as follows. In a 10-mL centrifuge tube were placed 3 mL of an aqueous potassium salt solution and 3 mL of chloroform containing a carrier, and the tube was shaken for 1 h at ambient temperature (25 ± 2 °C). The mixture was then allowed to stand overnight in a thermostat (25 ± 0.2 °C) and was centrifuged. The K^+ concentrations both in the aqueous phase and in the chloroform phase were determined by atomic absorption spectrophotometry. The measurement was repeated twice for each system, and the results agreed within ±2% for crown ethers and ±10% for PN. The distribution coefficients of crown ethers between the aqueous and chloroform phases were determined by the method of Frensdorff[9] at two concentrations between 0.01 and 0.1 mol dm^{-3} for a given crown ether. The values thus obtained were consistent within ±10%.

Results and Discussion

Extraction Equilibrium. When a univalent cation forms a 1:1 complex with a neutral ligand, the overall equilibrium between an aqueous phase containing an alkali metal cation (M^+) and a counteranion (A^-) and an organic phase containing a neutral ligand (L) can be written as in eq 1 where MLA denotes an ion

$$M^+_a + L_o + A^-_a \rightleftharpoons MLA_o$$

$$K_e = \frac{[MLA]_o}{[M^+]_a[L]_o[A^-]_a} \quad (1)$$

pair between the alkali-metal complex cation (ML^+) and A^-, subscripts a and o refer, respectively, to an aqueous phase and an organic phase, the square bracket means molarity, and K_e is the overall extraction constant.

Under the assumption that the complex ion pair hardly dissociates in the organic phase, the material balance is expressed by equations 2–4 where c denotes the total concentration of each

$$[M^+]_a = c_M^\circ - \bar{c}_M - [ML^+]_a - [MLA]_a \quad (2)$$

$$[A^-]_a = c_A^\circ - \bar{c}_A - [MLA]_a \quad (3)$$

$$[L]_o = \bar{c}_L^\circ - [L]_a - [ML^+]_a - [MLA]_a - [MLA]_o \quad (4)$$

species, superscript o refers to the initial concentration, and the bar over a symbol refers to the organic phase. If $[L]_a$, $[ML^+]_a$, and $[MLA]_a$ are negligibly small, as would be expected in the present experiments, eq 2–4 are reduced to eq 5–7. Substitution

$$[M^+]_a = c_M^\circ - \bar{c}_M = c_M \quad (5)$$

$$[A^-]_a = c_A^\circ - \bar{c}_A = c_M^\circ - \bar{c}_M = c_M \quad (6)$$

$$[L]_o = \bar{c}_L^\circ - [MLA]_o = \bar{c}_L^\circ - \bar{c}_M \quad (7)$$

of eq 5–7 into eq 1 gives the distribution ratio of the metal, $\bar{c}_M/c_M$, as in eq 8. Thus, the plot of log $\bar{c}_M/c_M$ vs. log $c_M(\bar{c}_L^\circ - \bar{c}_M)$ should

$$\bar{c}_M/c_M = K_e c_M(\bar{c}_L^\circ - \bar{c}_M) \quad (8)$$

give a straight line with a slope of unity and the intercept of which yields the equilibrium constant (K_e). Equation 8 can be rewritten as in eq 9. When the concentration of the metal salt is high,

$$\bar{c}_M = K_e\bar{c}_L^\circ c_M^2/(1 + K_e c_M^2) \quad (9)$$

molarity should be replaced by activity to obtain eq 10 where a is the activity of the salt in the aqueous phase and K_a' is the

$$\bar{c}_M = K_a'\bar{c}_L^\circ a^2/(1 + K_a' a^2) \quad (10)$$

conditional extraction constant as defined by Marcus and Asher.[14] The conditional extraction constant is defined by

$$K_a' = K_a\bar{y}_L/\bar{y}_{MLA}$$

$$K_a = \frac{\bar{c}_M\bar{y}_{MLA}}{a^2\bar{c}_L\bar{y}_L}$$

where $\bar{y}_{MLA}$ and $\bar{y}_L$ are, respectively, the activity coefficients of MLA and L in the organic phase, though these coefficients in chloroform are as yet unknown.

The K_e values determined from the log $\bar{c}_M/c_M$ vs. log $c_M(\bar{c}_L^\circ - \bar{c}_M)$ plots are listed in Table I. To date, the K_e values for K^+

(8) Yoshida, S.; Hayano, S. *J. Membr. Sci.* **1982**, *11*, 157–168.
(9) Frensdorff, H. K. *J. Am. Chem. Soc.* **1971**, *93*, 4684–4688.
(10) Sadakane, A.; Iwachido, T.; Toei, K. *Bull. Chem. Soc. Jpn.* **1975**, *48*, 60–63.
(11) Takeda, Y.; Goto, H. *Bull. Chem. Soc. Jpn.* **1979**, *52*, 1920–1922.
(12) Hasegawa, Y.; Wakabayashi, H.; Sakuma, M.; Sekine, T. *Bull. Chem. Soc. Jpn.* **1981**, *54*, 2427–2429.
(13) Buncel, E.; Shin, H. S.; Bannard, R. A. B.; Purdon, J. G.; Cox, B. G. *Talanta* **1984**, *31*, 585–592.
(14) Marcus, Y.; Asher, L. E. *J. Phys. Chem.* **1978**, *82*, 1246–1254.

Table I. Rates of Transport (J), Apparent Rate Constants of Ion Uptake (k_u) and Ion Release (k_r), and Overall Extraction Constants (K_e) for the Four Macrocyclic Carrier–Salt Combinations Examined

carrier	salt	J^a	$k_u{}^b$	$k_r{}^b$	$k_uK_e{}^c$	$K_e{}^d$
DB18C6	K^+Pic^-	3.0	11	15	41	3.70×10^4
DC18C6	K^+Pic	11.5	5.5	8.4	381	6.93×10^5
18C6	K^+Pic	13.7	9.4	11	754	8.02×10^5
PN	KSCN		5.7	5.1	0.34	6.0×10^2

[a] The source phase is water containing 1×10^{-3} mol dm^{-3} salt; the carrier concentration is 2×10^{-3} mol dm^{-3}; J is in 10^{-9} mol cm^{-2} min^{-1}. [b] In 10^{-4} cm s^{-1}. [c] In 10^6 cm^7 mol^{-2} s^{-1}. [d] In dm^6 mol^{-2}.

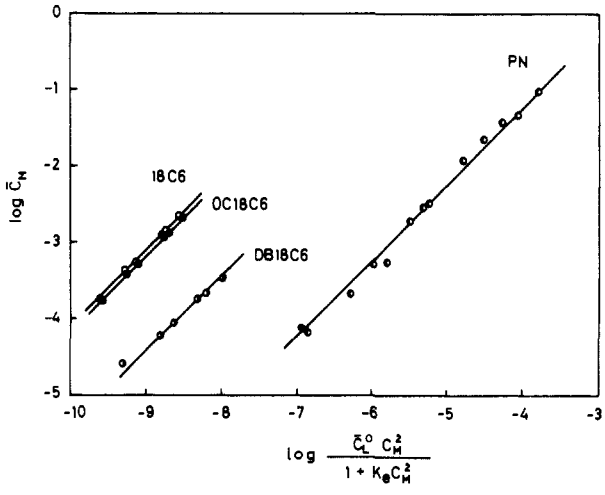

Figure 2. Plot of log $\bar{c}_M$ vs. log $\bar{c}_L{}^{\circ}c_M{}^2/(1 + K_ec_M{}^2)$. The salt employed is potassium picrate for crown ethers and KSCN for polynactin.

complexes of crown ethers other than DB18C6 have not been determined at the aqueous phase/chloroform interface, despite its frequent use in membrane transport experiments. The log K_e value obtained here for DB18C6 (4.57) agrees satisfactorily with the literature value (4.6).[12] The extractability of potassium is seen to be in the order DB18C6 ≪ DC18C6 < 18C6. Figure 2 shows the plots of log $\bar{c}_M$ against log $\bar{c}_L{}^{\circ}c_M{}^2/(1 + K_ec_M{}^2)$ for crown ethers and against log $\bar{c}_L{}^{\circ}a^2/(1 + K_a'a^2)$ for PN. The data points are well on a straight line with a slope of unity for each ligand; this demonstrates the validity of eq 9 and 10 in analyzing the partition of K^+ at the aqueous phase/membrane interface.

Ion Transfer across the Interface. Figure 3 depicts typical time courses for the ion uptake and the ion release. In each case, the K^+ concentration in the aqueous phase changes linearly with time at the early stage, and the rates of ion uptake, J_u, and of ion release, J_r, were calculated from the slope of the straight line. The J_u and J_r values obtained in two or three independent runs for a given system agreed with each other within ±10%.

We then examined quantitatively the effect of potassium salt concentration on the rates of ion uptake and ion release by varying its concentration in the source phase (the aqueous phase for uptake and the chloroform phase for release). Figure 4 illustrates the dependence of the uptake rate (J_u) on the salt concentration. For potassium picrate–crown ether systems, log J_u values are plotted against log c_M (molarity) since c_M is limited to a sufficiently low range. In all cases, the points at lower a or c_M are on straight lines having a slope of 2. However, a negative deviation from the line is noted at higher a or c_M. To elucidate these findings, we develop in what follows the kinetic equations for the ion uptake and the ion release.

If the diffusion of a metal–carrier complex in the membrane solution phase is the rate-determining step for the ion transfer across the interface, the rate of ion transfer should be proportional to the concentration gradient in the membrane solution phase as in eq 11 and 12 where k_u and k_r are defined as the apparent rate

$$J_u = k_u(\bar{c}_M{}^* - \bar{c}_M) \tag{11}$$

$$J_r = k_r(\bar{c}_M - \bar{c}_M{}^*) \tag{12}$$

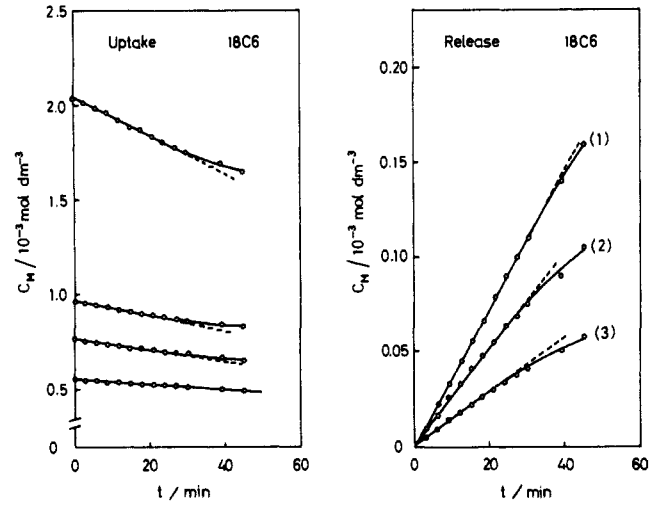

Figure 3. Temporal evolution of the K^+ concentration (c_M) in the aqueous phase for ion uptake and ion release by 18C6. The concentration of 18C6 in the chloroform phase is 2×10^{-3} mol dm^{-3}. Initial concentrations (mol dm^{-3}) of the K^+-18C6 complex in the chloroform phase are (1) 1.1×10^{-3}, (2) 5.2×10^{-4}, and (3) 2.6×10^{-4}.

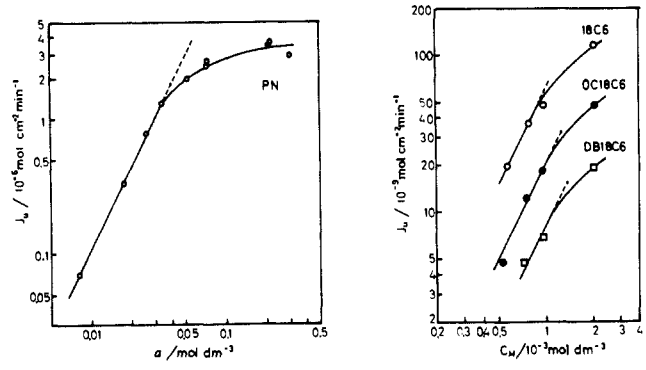

Figure 4. Dependence of the rate of K^+ uptake by polynactin (0.1 mol dm^{-3} in the chloroform phase) and by crown ethers (2×10^{-3} mol dm^{-3} in the chloroform phase) on the KSCN activity and potassium picrate molarity in the aqueous phase, respectively.

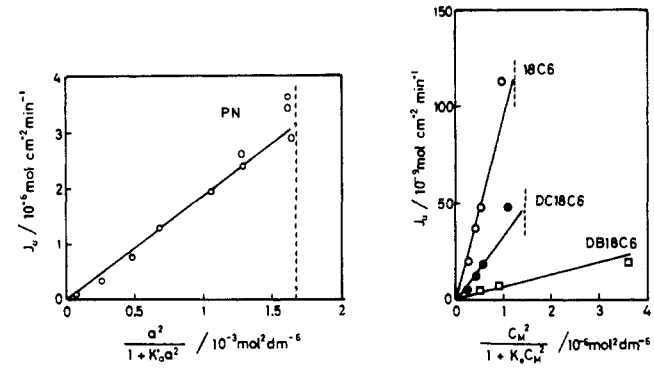

Figure 5. Left: J_u vs. $a^2/(1 + K_a'a^2)$ plot for the polynactin–KSCN system. Right: J_u vs. $c_M{}^2/(1 + K_ec_M{}^2)$ plots for the crown ether–potassium picrate systems.

constants of uptake and release, respectively, and the asterisk indicates the concentration at the interface. In the case where the complexation readily attains an equilibrium at the interface, $\bar{c}_M{}^*$ is related to the concentration in the aqueous phase by eq 9 or 10. Since $\bar{c}_M$ is negligibly low at the early stage of ion uptake, eq 11 is reduced to eq 13 and 14. Similarly, since $\bar{c}_M - \bar{c}_M{}^* \approx$

$$J_u = k_uK_e\bar{c}_L{}^{\circ}\frac{c_M{}^2}{1 + K_ec_M{}^2} \tag{13}$$

$$J_u = k_uK_a'\bar{c}_L{}^{\circ}\frac{a^2}{1 + K_a'a^2} \tag{14}$$

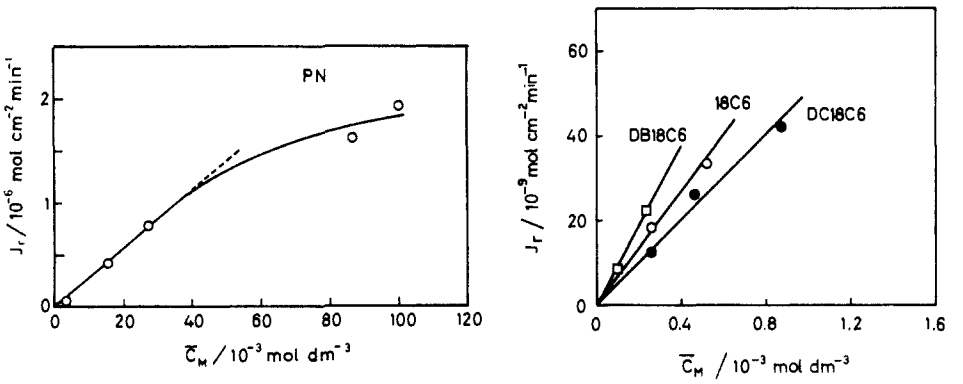

Figure 6. Relationship between the release rate and the complex concentration in the chloroform phase. Left: polynactin–KSCN system; [PN] = 0.1 mol dm^{-3}. Right: crown ether–potassium picrate systems; [crown ether] = 2 × 10^{-3} mol dm^{-3}.

$\bar{c}_M$ at the early stage of ion release, eq 12 is approximated by eq 15. As seen in Figure 5, the plot of J_u vs. $c_M^2/(1 + K_e c_M^2)$ or

$$J_r = k_r \bar{c}_M \tag{15}$$

J_u vs. $a^2/(1 + K_a' a^2)$ indeed gives a straight line over a wide range of salt concentrations in the aqueous phase. The negative deviation depicted in Figure 4 could thus be explained by invoking that the term $K_e c_M^2$ in eq 13 or $K_a' a^2$ in eq 14 is no longer negligible with respect to 1 at higher salt concentration. As c_M increases, the term $c_M^2/(1 + K_e c_M^2)$ asymptotes to a maximum, $1/K_e$. If all other terms in eq 13 or 14 are constant, J_u should approach a constant value with increasing c_M. The $1/K_e$ values for three potassium–carrier combinations are indicated by broken lines in Figure 5.

On the other hand, J_r increased linearly with an increase in the concentration of the metal–carrier complex in the membrane solution phase (Figure 6), as expected from eq 15. The negative deviation from the straight line at higher $\bar{c}_M$ for the PN system may be a consequence of plotting J_r against molarity instead of against activity. The activity of the complex in chloroform is unknown. We can thus evaluate the rates of ion uptake and ion release from the slope of the straight lines in Figures 5 and 6; the slope is $k_u K_e$ for ion uptake and k_r for ion release. The kinetic parameters determined in this manner are summarized in Table I.

For each carrier system, the k_r value is comparable to the k_u value, so that the ion release is not the rate-limiting step. These values are of the order of D/l calculated from the diffusion coefficient (D, 10^{-5} cm^2 s^{-1}) and the thickness of the Nernst layer (l, 50–300 μm); $D/l \approx$ (4–20) × 10^{-4} cm s^{-1}.[7] Thus, a diffusion-limited process is compatible with the present experimental data. The variation of the J value among the three crown ethers, DB18C6 < DC18C6 < 18C6, parallels that of the $k_u K_e$ value; the rate of transport hence depends on the parameter $k_u K_e$. The extractability of a metal ion makes a relatively large contribution to the magnitude of $k_u K_e$. For a higher extractability, the concentration gradient of the metal–carrier complex in the membrane phase is steeper, so that the rates of uptake and transport should increase as K_e increases.

The overall extraction equilibrium can be analyzed in terms of the following constituent equilibria.[10]

$$K_{dL} = \frac{[L]_o}{[L]_a}$$

$$K_s = \frac{[ML^+]_a}{[M^+]_a[L]_a}$$

$$K_{MLA} = \frac{[MLA]_a}{[ML^+]_a[A^-]_a}$$

$$K_{dMLA} = \frac{[MLA]_o}{[MLA]_a}$$

The overall extraction equilibrium constant (K_e) is given by eq 16. As in a foregoing argument, the dissociation of the complexed ion pair (MLA) in the organic phase into ML^+_o and A^-_o is excluded. The values of K_{dL}, K_s, and K_e' as well as K_e are listed in Table II.

Table II. Equilibrium Constants for Extraction of Potassium with Macrocyclic Ligands

ligand	salt	log K_e	log K_{dL}	log K_s	log K_e'	log K_e'/K_{dL}
DB18C6	K^+Pic^-	4.57	3.9[a]	1.67[b]	6.8	2.9
DC18C6	K^+Pic^-	5.84	3.1	1.83[c]	7.1	4.0
18C6	K^+Pic^-	5.90	0.94	2.06[d]	4.78	3.84
PN	KSCN	2.78				

[a] From ref 12. [b] From ref 18. [c] Average of log K_s values for isomers A and B; from ref 19. [d] From ref 20.

$$K_e = \frac{K_s K_{MLA} K_{dMLA}}{K_{dL}} = \frac{K_s K_e'}{K_{dL}} \tag{16}$$

The magnitude of K_e for crwon ethers is governed primarily by that of the stability constant (K_s). The distribution coefficient (K_{dL}) of DB18C6 is roughly 10^4-fold greater than that of 18C6; DB18C6 is much more hydrophobic than 18C6. The hydrophobicity of a ligand shows virtually no effect on the stability of the complex, but it does have a slight effect on K_e. The magnitude of K_e is also governed by that of K_e'/K_{dL} (cf. eq 16). Although DB18C6 is superior to 18C6 in extractability (K_e') of the metal–ligand complex, the K_e'/K_{dL} value for DB18C6 is smaller than that for 18C6. This originates from a very high K_{dL} value of DB18C6. In other words, the low K_{dL} of 18C6 raises the K_e'/K_{dL} value and enhances the extractability of the metal ion. The K_e'/K_{dL} value for DC18C6 is higher than that for DB18C6 because of the lower hydrophobicity of the former. Thus, the lower hydrophobicity of a ligand as well as the stability of the resulting complex leads to an enhancement in the extractability of the metal ion. These results indicate that a ligand forming a more stable complex with the metal ion and moreover being less hydrophobic is preferable as a mobile carrier in liquid membrane systems.

Ion Transport through Liquid Membrane. Figure 7 shows the rate of potassium transport by PN as a function of $a^2/(1 + K_a' a^2)$. The rate of transport increases linearly with an increase in $a^2/(1 + K_a' a^2)$. This result is in accordance with the eq 17 as described by several authors[2-4,6] where k is the apparent rate constant of

$$J = kK_a' \bar{c}_L{}^o \frac{a^2}{1 + K_a' a^2} \tag{17}$$

transport through a liquid membrane. No previous workers were able to quantify the apparent rate constant (k) because the parameter K_a' had not been properly evaluated. The value of k, obtained by introducing the presently determined K_a' for PN into eq 17, is 1.2 × 10^{-4} cm s^{-1}. This is, however, smaller than the theoretically expected $k_u/2$ value (2.8 × 10^{-4} cm s^{-1}).[15] This

(15) If the boundary layers on both sides of the membrane are equal in thickness, the k value should be equal to half the apparent rate constant determined in the uptake or release experiment.

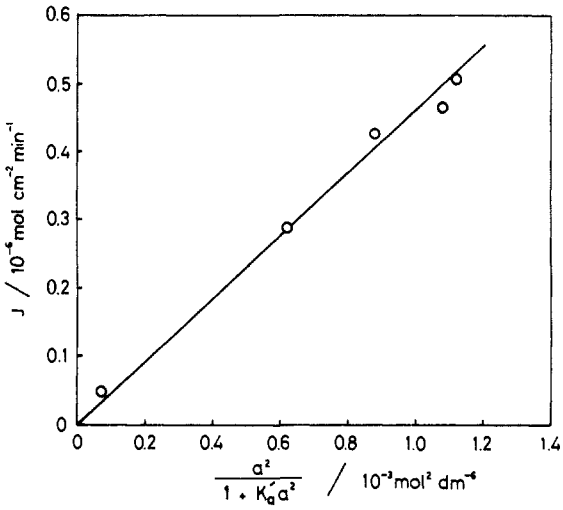

Figure 7. J vs. $a^2/(1 + K_a'a^2)$ plot for the polynactin-KSCN system. [PN] = 0.1 mol dm^{-3}.

discrepancy may be due to a difference in the stirring conditions between the ion-transfer and ion-transport experiments. If the two experiments could be carried out under the same stirring conditions, a theoretical curve for ion transport might be drawn by use of the apparent rate constant derived from ion-transfer experiments.

For all the carriers studied here, the value of k_r is comparable to that of k_u, so that the rate of release does not control the overall rate of transport. When log K_e is higher than 4–6 for a monovalent cation, the rate of transport decreases with an increase in K_e as demonstrated by Behr and co-workers.[7] The rate of release decreases with an increase in the stability constant of the complex and controls the rate of transport in the region of high stability.[16] When K_e is very high, the concentration of the complex at the interface on the release side ($\bar{c}_M$*) is not longer negligible in comparison with the concentration in the bulk solution ($\bar{c}_M$). Under these circumstances, we have to use eq 12, or $J_r = k_r'\bar{c}_M$ where $k_r' = k_r(1 - \bar{c}_M^*/\bar{c}_M)$; the k_r' apparently decreases with an increase in $\bar{c}_M$*. The k_r' values, calculated from J_r values previously determined for potassium picrate,[16,17] were 0.27×10^{-4} and 0.82×10^{-4} cm s^{-1} for cryptand 2.2.2 and dibenzocryptand 2.2.2, respectively. These values are 1–2 orders of magnitude lower than those for crown ethers. In such a case, the transport of the ion does not proceed so fast as would be expected from its high affinity to the carrier. However, most of the metal complexes with macrocyclic ligands exhibit log K_e of 4–6 or lower,[10-13] so that the rate of transport is predictable from the extractability of the metal ion.

Acknowledgment. We are grateful to Chugai Pharmaceutical Co., Ltd., for kindly supplying us with polynactin, and to H. Inoue, T. Takahashi, and S. Tanaka for their assistance in the experiments.

(16) Yoshida, S.; Hayano, S. *J. Membr. Sci.* **1986**, *26*, 99–106.
(17) When $\bar{c}_M$ was 1×10^{-3} mol dm^{-3}, the J_r values were 1.6×10^{-9} and 4.9×10^{-9} mol min^{-1} cm^{-2} for cryptand 2.2.2 and dibenzocryptand 2.2.2, respectively.
(18) Shchori, E.; Nae, N.; Grodzinski, J. J. *J. Chem. Soc., Dalton Trans.* **1975**, 2381–2386.
(19) Izatt, R. M.; Nelson, D. P.; Rytting, J. H.; Haymore, B. L.; Christensen, J. J. *J. Am. Chem. Soc.* **1971**, *93*, 1619–1623.
(20) Frensdorff, H. K. *J. Am. Chem. Soc.* **1971**, *93*, 600–606.

Analysis of the Absorption and Fluorescence Spectra of Trimethylamine: Determination of the $\tilde{A}$–$\tilde{X}$ Origin and the Ground-State Inversion Barrier

Arthur M. Halpern,* Mary Jo Ondrechen, and Lawrence D. Ziegler

Contribution from the Department of Chemistry, Northeastern University, Boston, Massachusetts 02115. *Received December 26, 1985*

Abstract: The second derivative of the gas-phase absorption spectrum of trimethylamine (TMA) is used to assign the positions of many vibrational features in the $\tilde{A} \leftarrow \tilde{X}$ transition. Considerable regularity in these positions indicates that the $\tilde{A}$ state potential is harmonic in the out-of-plane bending coordinate, and a frequency of 375 cm^{-1} is assigned. Calculations based on the finite difference method using an $\tilde{X}$-state inversion potential of local harmonic wells joined by a parabolic or quartic cap and a harmonic $\tilde{A}$ state are successfully used to fit the shapes of both the absorption and fluorescence spectra. Most of the Franck–Condon activity in fluorescence involves transitions to the $v'' = 14$–18 states, explaining the large Stokes' shift as well as the vertical shape. The origin of the $\tilde{A} \leftarrow \tilde{X}$ transition is assigned at 37 550 cm^{-1}, and the inverion barrier height is estimated to be 2900 cm^{-1} based on a parabolic- or quartic-capped pair of harmonic wells. Comparisons are made with calculated TMA inversion barriers.

Electronic transitions between potential energy surfaces that are severely distorted and displaced from each other serve as a sensitive probe of the characteristics of these surfaces. Thus absorption and emission band shapes can reveal detailed information about potential energy surfaces possessing multiple minima which are ubiquitous in applications to chemical structure and reactivity. One classic example concerns the ground and excited electronic states of ammonia, the former of which is characterized by the well-known double minimum inversion potential. The pyramidal to planar structural change that accompanies electronic excitation in ammonia lends a degree of richness and complexity to its spectroscopy that has been the focus of intense interest from the microwave to the UV region for many years.[1] The same fundamental structural properties that attend to the upper and lower electronic states in ammonia apply as well to trimethylamine

(1) (a) Douglas, A. E. *Discuss. Faraday Soc.* **1963**, *35*, 158. (b) Walsh, A. D.; Warsop, P. A. *Trans. Faraday Soc.* **1961**, *57*, 345. (c) Ziegler, L. D.; Hudson, B. *J. Phys. Chem.* **1984**, *88*, 1110. (d) Vaida, V.; Hess, W.; Roebber, J. L. *J. Phys. Chem.* **1984**, *88*, 3397.

0002-7863/86/1508-3907$01.50/0